



## ORIGINAL ARTICLE

# Inhibitory effect of protonic bis(5-amino-1,10-phenanthroline) on proliferation of hepatocellular carcinoma and its molecular mechanism



Zizhen Zhao, Chen Fu, Yuping Zhang, Yingying Zhang, Xiaoxi Yang, Ailing Fu\*

College of Pharmaceutical Science, Southwest University, Chongqing 400715, China

Received 14 December 2021; accepted 17 May 2022

Available online 21 May 2022

## KEYWORDS

Hepatocellular carcinoma;  
Protonic bis-phenanthroline;  
PLAGL2;  
Apoptosis;  
Hydrogen bond

**Abstract** The incidence of HCC continues to increase rapidly in recent years. The principle of developing anti-HCC drugs is to specifically kill tumor cells, without affecting the function of normal cells. Here we synthesized a novel protonic compound bis(5-amino-1,10-phenanthroline) (P-BAP), and the antitumor activity was explored *in vitro* and *in vivo*. The results showed that P-BAP could selectively inhibit the proliferation of tumor cells, and induce HCC apoptosis. In HCC-bearing mice, P-BAP could effectively retard the tumor growth, even completely eliminate the tumors at the dose of 5 mg/kg, and meanwhile P-BAP had no significant effect on mouse body weight. Mechanism analysis revealed that P-BAP could down-regulate the protein expressions of pleomorphic adenoma gene like-2 (PLAGL2), HIF-1 $\alpha$  and  $\beta$ -catenin, and up-regulate the levels of pro-apoptotic protein BAX and BNIP3. In addition, P-BAP could reduce mitochondrial respiratory chain complex activities, leading to insufficient ATP production. The study provides a new approach for designing selective antitumor drugs, and suggests that P-BAP would be a potential candidate for HCC therapy.

© 2022 The Authors. Published by Elsevier B.V. on behalf of King Saud University. This is an open access article under the CC BY-NC-ND license (<http://creativecommons.org/licenses/by-nc-nd/4.0/>).

## 1. Introduction

Hepatocellular carcinoma (HCC) is one of the most common cancer with high mortality worldwide. The main risks causing HCC include viral hepatitis, alcoholic cirrhosis and nonalco-

holic steatohepatitis (Adams et al., 2020; Torre et al., 2021). Patients with early HCC always have no obvious clinical symptoms, however, with the disease progress and deterioration of liver function, most of patients lose the opportunity of surgical resection and liver transplantation, and have to accept the systemic medication. In clinic, systemic therapy is particularly important for the patients with high-risk and advanced HCC (Anwanwan et al., 2020; Chen et al., 2020). Therefore, it's urged to develop anti-HCC drugs with high efficiency and low toxicity.

In the designing and synthesizing anti-HCC drugs, we take into account hydrogen-bonded compounds because hydrogen bond is the most basic and extensive chemical bond in bio-

\* Corresponding author.

E-mail address: [fal@swu.edu.cn](mailto:fal@swu.edu.cn) (A. Fu).

Peer review under responsibility of King Saud University.



organisms (Karas et al., 2020; Vladilo and Hassanali, 2018). Hydrogen bond widely participates in biochemical reactions and life activities such as molecular recognition, expression of genetic information, regulation of metabolic processes, and so on. Generally, hydrogen bond energy lies in between covalent bond and non-covalent bond. But it's reported that under certain condition, stable chemicals conjugated with strong hydrogen bond can be formed between molecules (Karas et al., 2020; Vladilo and Hassanali, 2018). Thus, we connected two 5-amino-1,10-phenanthroline through the synthetic technology of hydrogen-bonded dimerization to form a stable protonic bis(5-amino-1,10-phenanthroline) (P-BAP) compound. The application of hydrogen-bonded dimerization may provide a new approach for the development of drugs.

To identify the biological activity and cell selectivity of P-BAP, several tumor cells (including HCC) and normal cells were used in the study. Moreover, it's reported that pleomorphic adenoma gene like-2 (PLAGL2), a proto-oncogene transcription factor, is involved in HCC cell proliferation and metastasis *in vitro* and *in vivo* (Hu et al., 2021; Wang et al., 2021), and PLAGL2 contributes to mitochondrial function and increases mitochondrial apoptosis resistance in HCC cells (Yang et al., 2021; Zhao et al., 2022). Therefore, both PLAGL2 level and mitochondrial function were examined in the study to identify the anti-HCC mechanism of P-BAP. The study might provide a potential candidate for HCC therapy.

## 2. Experimental section

### 2.1. Experimental reagents and materials

The cell lines, including human non-small cell lung cancer cell line (A549 cell), mouse liver cancer cell line (H22 cell), human glioma cell line (U251 cell), normal human liver cell line (L02 cell), and human embryonic kidney 293 cell line (HEK 293 cells) from ATCC, were stored in our laboratory (Zhang et al., 2019). Ammonium hexafluorophosphate ( $\text{NH}_4\text{PF}_6$ ; CAS16941-11-0), 5-amino-1,10-phenanthroline (CAS 54258-41-2), and other chemical reagents were purchased from Shanghai Aladdin Biochem. Tech. Co. Ltd. (China). Antibodies against  $\beta$ -actin (Catalog. GB11001), HIF-1 $\alpha$  (Catalog. GB13031-1),  $\beta$ -catenin (Catalog. GB11015) and horse radish peroxidase (HRP)-labeled goat anti-rabbit secondary antibody were obtained from Wuhan Servicebio. Biotech. Co. Ltd. (China), and pleomorphic adenoma gene like-2 (PLAGL2) antibody (Catalog. D162056), Bax antibody (Catalog. D197138) and Bcl-2 nineteen kilodalton interacting protein 3 (BNIP3) antibody (Catalog. D221876) were from Shanghai Sangon Bioeng. Co. Ltd. (China). Cell counting kit-8 (CCK-8; Catalog. C0040) and TdT-mediated dUTP nick end labeling (TUNEL) apoptosis kit (Catalog. C1086) were purchased from Beyotime Biotech. Co. Ltd. (China). Cell culture reagents and materials were purchased from GIBCO Co. (USA).

### 2.2. Synthesis of P-BAP

The 5-amino-1,10-phenanthroline (1.0 g, 5.12 mmol) was dissolved in 10 mL aqueous-alcohol solution with equivoluminal distilled water and ethanol, then ten equivalents of  $\text{NH}_4\text{PF}_6$  was added to the reaction flask under a nitrogen atmosphere.

The mixture was stirred for 2 h at room temperature, and it was then evaporated to dryness. The resulting solid was dissolved in 10 mL acetonitrile, filtered, and the insoluble was abandoned. Then desired P-BAP product with pure orange color was obtained by freeze-drying of the filtrate (yield 1.10 g; productivity  $\sim$  80%). The melting point of the compound was determined using a melting-point tester. The chemical structure of the compound was characterized by Fourier transform infrared spectroscopy (FTIR; Thermo Scientific Nicolet), nuclear magnetic resonance spectroscopy (NMR; Bruker Avance NEO), and high-resolution mass spectrometry (HRMS; Finnigan LTQ-FT instrument). The purity of the product was measured by high performance liquid chromatography (HPLC; Shimadzu, Japan).

### 2.3. Measurements of cell viability and apoptosis

H22 cells in logarithmic growth stage were cultured on 96-well plates for cell viability assay. When cell confluency reached 80  $\sim$  90%, P-BAP was dissolved in phosphate-buffered saline (PBS) with the concentration of 1.56, 3.12, 6.25, 12.5, 25, 50, 100, 200  $\mu\text{mol/L}$  respectively and then was added to the culture media. The same concentrations of cisplatin and 5-amino-1,10-phenanthroline were respectively added into the media as the controls. The same volume of PBS was added as the negative control. After addition, the culture plates were placed in cell incubator for 24 h, and then the cell viability was measured by CCK-8. The absorbance at 450 nm was detected on a spectrophotometer. The cell viability was calculated as  $[(A_{\text{sample}} - A_{\text{blank}})/(A_{\text{control}} - A_{\text{blank}})] \times 100\%$ .

Cell apoptosis was measured by TUNEL staining according to the manufacture's manual (Shanghai Beyotime Biotech. Co. Ltd., China). After 12.5  $\mu\text{mol/L}$  P-BAP was added into the six well plates for 24 h incubation, the cells were stained by the TUNEL staining kit. The cells were observed under a fluorescence microscope (Olympus, Japan).

### 2.4. Western blot (WB)

Cells were collected and put into RIPA cell lysis solution for 30 min in ice bath. Then the solution was centrifuged at 10,400 g for 5 min. The supernatant was taken for SDS-PAGE. After the samples were transferred to polyvinylidene fluoride (PVDF) membrane, the membrane was sealed by 5% skimmed milk powder for 2 h, and then respectively incubated with primary antibodies of PLAGL2, HIF-1 $\alpha$ ,  $\beta$ -catenin, Bax, BNIP3 and  $\beta$ -actin overnight. Following washed by Tris-buffered saline with 0.1% Tween 20 (TBST) for 3 times, the membrane was incubated with goat anti-rabbit secondary antibody labeled with HRP at room temperature for 90 min. After the membrane was washed with TBST, enhanced chemiluminescence (ECL) imaging system was used for developing and photographing images (Shanghai Qinxiang Sci. Instru. Co., Ltd., China).

### 2.5. Biochemical assay

Activities of mitochondrial respiratory chain complex I, II and IV were respectively detected by using the commercial kits (Sinobestbio. Tech. Co. Ltd., China). ATP content was also

measured according to commercial kit's protocol (Suzhou Grace Biotech. Co., China).

### 2.6. Animals

Healthy male ICR mice were obtained from Chongqing Enswell Anim. Sci. Tech. Co., Ltd., and fed in the Animal Center of Southwest University of specific pathogen free (SPF) grade. The mice are raised under the standard condition. Mice aged 1.5 months were used to prepare subcutaneous tumor model. The experimental protocols were approved by the Animal Ethics Committee of Southwest University (IACUC-20210215-04).

### 2.7. Preparation of tumor-bearing mice and P-BAP treatment

H22 cells in logarithmic growth stage were collected and washed by PBS, then the cells were suspended in PBS. The cell suspension was subcutaneously transplanted to the right axillary of mice ( $10^7$  cells/mouse). Following injection for 3 days, obvious tumor mass would appear. The tumor volume gradually increased with days. The volume increased to about  $0.3 \text{ cm}^3$  [Tumor volume ( $\text{cm}^3$ ) =  $0.5 \times L \times D^2$ ; L, tumor long side; D, tumor short side], measured by vernier caliper, then the tumor-bearing mice were randomly divided into 5 groups with 8 mice in each group. In P-BAP treatment group, P-BAP with doses of 2.5 mg/kg (low dose group), 5 mg/kg (medium dose group) and 10 mg/kg (high dose group) were respectively injected intravenously to the mice once a day for 10 days. The mice in positive control group were given 10 mg/kg cisplatin intravenously. The model control group was given the same volume of saline. After the tumor volume in the model group arrived to about  $3.0 \text{ cm}^3$ , all mice were euthanatized, and the tumors were respectively dissected out and weighed.

### 2.8. Tissue staining

Tumor mass in each group were respectively fixed with 4% paraformaldehyde, embedded in paraffin, sectioned and stained with HE. In addition, Tumor mass were routine frozen section, and immunohistochemical staining was performed with TUNEL apoptosis reagent according to the manufacturer's protocol. The slices were observed under the fluorescence microscope.

### 2.9. Statistical analysis

The data were expressed as mean  $\pm$  standard deviation (mean  $\pm$  SD). The data were statistically analyzed using GraphPad Prism 7.0. Student's test (T-test) was used to evaluate the difference between the two groups of samples, and one-way ANOVA was used to compare the differences between multiple groups of samples. Statistical  $p < 0.05$  indicated that the difference is statistically significant between groups, and  $p < 0.01$  represented that the difference is highly statistically significant.

## 3. Results

### 3.1. Synthesis of P-BAP

P-BAP is synthesized through intermolecular proton transfer method,<sup>[7]</sup> in which one H of ammonium in  $\text{NH}_4\text{PF}_6$  is transferred to the N atoms of two 5-amino-1,10-phenanthroline to form the hydrogen bond of  $\text{N-H}^+ \cdots \text{N}$  (Fig. 1A). The structure of P-BAP was identified by  $^1\text{H}$  NMR,  $^{13}\text{C}$  NMR, FTIR, and HRMS, respectively (Fig. S1 and Fig. 1B). As shown in Fig. S1,  $^1\text{H}$  NMR (400 MHz, DMSO):  $\delta$  9.14 (m, 5H), 8.83–8.81 (d,  $J = 8.3$  Hz, 5H), 8.72 (d,  $J = 4.6$  Hz, 5H), 8.34 (d,  $J = 8.2$  Hz, 5H), 7.88 (dd,  $J = 8.3, 4.3$  Hz, 5H), 7.72 (dd,  $J = 8.3, 4.6$  Hz, 5H), 7.18 (s, 1H), 7.05 (s, 1H), 6.94 (s, 5H), 1.22 (s, 2H);  $^{13}\text{C}$  NMR (101 MHz, DMSO):  $\delta = 150.26, 146.07, 141.11, 139.32, 138.85, 133.57, 132.57, 130.65, 125.16$  (d,  $J = 15.7$ ), 122.81, 99.94. The FTIR spectrum shows that the compound possesses a strong hydrogen bond spectral peak between 3500 and 3000 nm (Fig. S1). HRMS calcd for  $\text{C}_{24}\text{H}_{18}\text{N}_6$  ( $\text{M} + \text{H}^+$ ): 391.1666, found 391.1663;  $\text{C}_{24}\text{H}_{18}\text{N}_6$  ( $\text{M} + \text{Na}^+$ ) 413.1485, found: 413.1484 (Fig. 1B). The purity of the obtained P-BAP is 99.7%, determined by HPLC (Fig. 1C). In addition, the melting point of the P-BAP is 367–369 °C, about 110 °C higher than that of raw material 5-amino-1,10-phenanthroline (254–258 °C).

### 3.2. P-BAP selectively inhibited tumor cell proliferation

To examine the tumor cell selectivity of P-BAP, three different tumor cell lines (H22 cell, A549 cell, and U251 cell) and two normal cell lines (L02 cell and HEK 293 cell) were used in the study. After P-BAP was added to the media of tumor cells, the effect of P-BAP on the tumor cell proliferation was respectively measured. The results showed that P-BAP could inhibit the three types of tumor cell proliferation in dose-dependent manners (Fig. 2A). The IC50 values of P-BAP were 5.8  $\mu\text{mol/L}$  (H22 cells), 6.4  $\mu\text{mol/L}$  (A549 cells) and 14.6  $\mu\text{mol/L}$  (U251MG cells) respectively after the tumor cells were treated with P-BAP. However, after P-BAP was added to the media of human normal liver cells and HEK 293 cells, the cell viabilities did not exhibit significant changes (Fig. 2B), suggesting that P-BAP could selectively inhibit tumor cell proliferation. In addition, when cisplatin and 5-amino-1,10-phenanthroline were respectively added into the cell media, the viabilities reduced in both tumor cells (H22 cells, A549 cells and U251 cells) and normal cells (L02 liver cells and HEK293 cells) (Fig. S2). Compared with the tumor cells, 5-amino-1,10-phenanthroline is more toxic to the normal cells.

Moreover, cell morphology was observed under an optical microscope after P-BAP addition. Compared to the control cells, the P-BAP-treated H22 cells became small and shrunken (Fig. 2C), which are the typical features of cell apoptosis. Then the cells were stained by TUNEL apoptosis reagent FITC-dUTP for apoptosis assay. The result showed that a large number of apoptosis-positive cells appeared after P-BAP treatment (Fig. 2D), indicating that P-BAP inhibited the cell proliferation though inducing cell apoptosis.

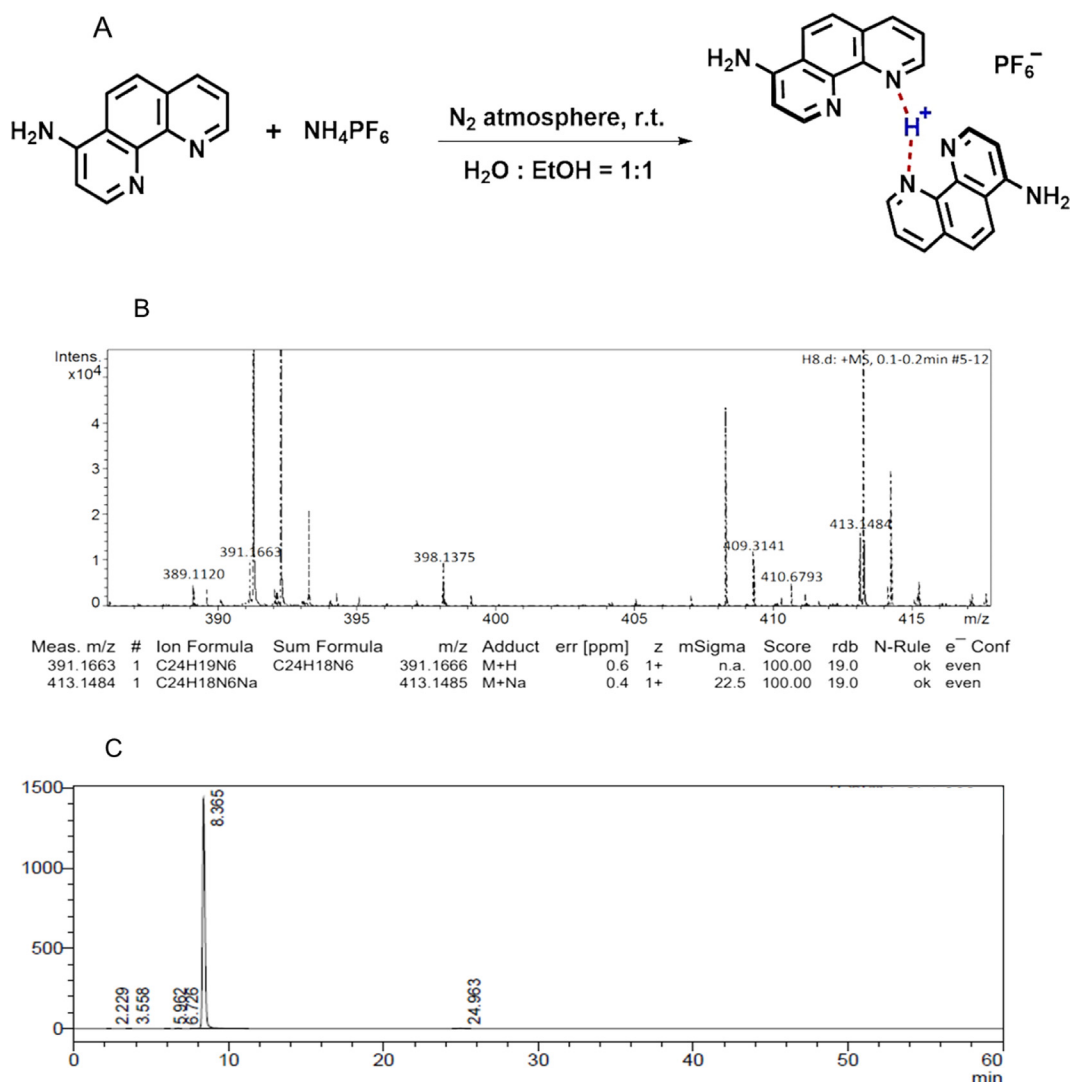


**Fig. 1** Synthesis and characteristic of P-BAP. (A) Synthesis process of P-BAP. (B) The chemical was identified by HRMS. (C) Purity of P-BAP was analyzed by HPLC. The chromatographic condition was as follows: Shim-pack Scepter C18-120 column ( $4.6 \times 250$  mm,  $5 \mu\text{m}$ ); mobile phase acetonitrile/water 20:80 (V/V), pH 6.0; flow rate 1.0 mL/min; detection wavelength 273 nm; column temperature  $25^\circ\text{C}$ ; injection volume 10  $\mu\text{L}$ .

### 3.3. P-BAP regulated the expression of PLAGL2 and related proteins

In order to clarify the molecular mechanism of P-BAP selectively inducing apoptosis of the tumor cells, proto-oncogene transcription factor PLAGL2 and its downstream regulatory proteins were examined by WB. The PLAGL2 expression levels in cells were respectively examined, and the result showed that PLAGL2 could be highly expressed in H22 cells, U251 cells and A549 cells, while few expressions were exhibited in L02 cells and HEK293 cells (Fig S3). After P-BAP treatment, the expressions of PLAGL2 were down-regulated in the tumor cells (Fig. S3). When P-BAP was added into the culture media of H22 cells for 30 min, the level of PLAGL2 protein decreased dramatically, and consistently reduced with time (Fig. 3A and 3B). The levels of related downstream proteins of PLAGL2, HIF-1 $\alpha$  and  $\beta$ -catenin, significantly reduced

accordingly (Fig. 3A, 3C, 3D). However, the levels of proapoptotic proteins BNIP3 and Bax that were closely associated with PLAGL2, increased significantly (Fig. 3A, 3E and 3F). The results suggest that P-BAP could inhibit the tumor cell proliferation and induce apoptosis through down-regulating the expression levels of PLAGL2, HIF-1 $\alpha$  and  $\beta$ -catenin, and up-regulating the pro-apoptotic proteins.

### 3.4. P-BAP could decrease energy supply

Since mitochondria play crucial roles in growth and proliferation of HCC (Altieri, 2017; Facciorusso et al., 2016; Keerthiga et al., 2021), activities of mitochondrial respiratory chain complexes and ATP content were respectively examined. The results were shown in Fig. 4A-C. The activities of mitochondrial complex I, II, IV of the tumor cells reduced in concentration-dependent pattern after P-BAP treatment at

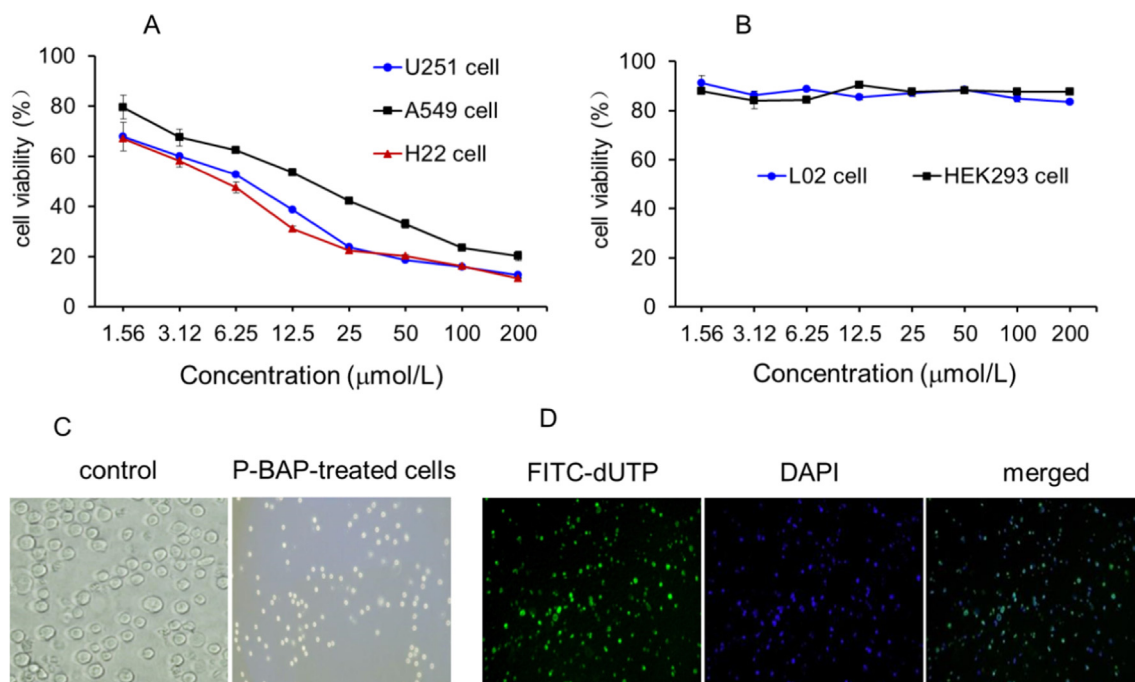


**Fig. 2** P-BAP inhibited tumor cell proliferation and induced H22 cell apoptosis. (A) P-BAP could inhibit U251 glioma cell, lung cancer A549 cells and liver cancer H22 cells in concentration-dependent manners. (B) P-BAP had few effects on the cell proliferation of human L02 hepatocytes and human embryonic kidney 293 (HEK293) cells. (C) Morphological changes of H22 cells after 12.5  $\mu\text{mol/L}$  P-BAP treatment for 24 h. (D) Numbers of apoptosis-positive cells appeared after P-BAP treatment, stained by FITC-dUTP (green) under fluorescence microscope. The nuclei were stained with DAPI (blue).

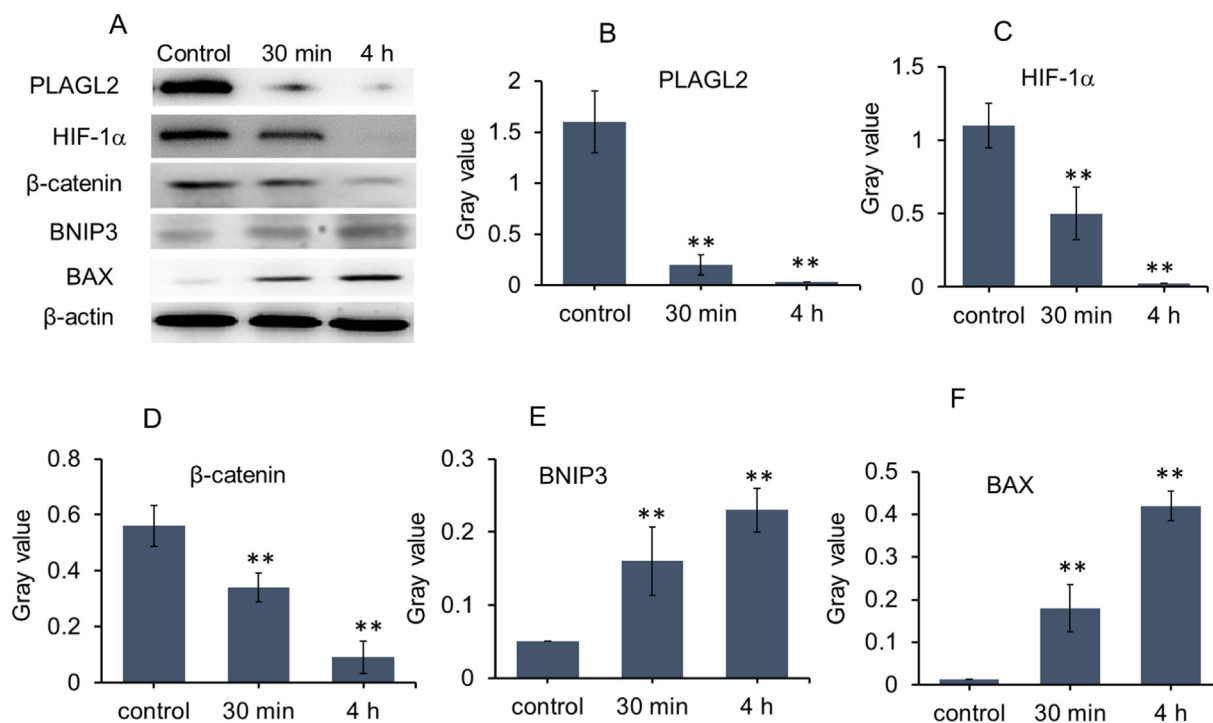


**Fig. 3** P-BAP could rapidly regulate the expression of PLAGL2 and related downstream molecules. (A) Protein levels after P-BAP (12.5  $\mu\text{mol/L}$ ) was added into cell media for 30 min and 4 h, evaluated by WB. (B-F) Gray value of WB (n = 3). The data were expressed by mean  $\pm$  SD. Compared to the control, \*\* $p < 0.01$  represented very significant difference.

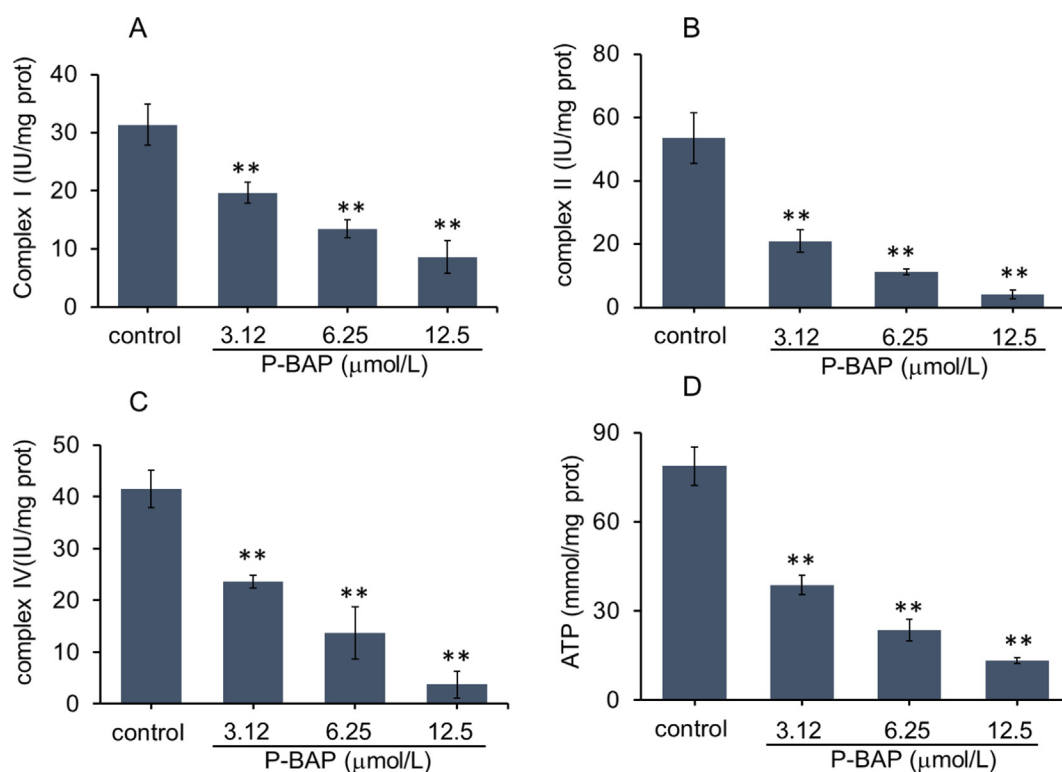


**Fig. 4** P-BAP could decrease mitochondrial respiratory function. (A-C) Activities of mitochondrial respiratory chain complex I, II, IV and (D) ATP content in liver cancer H22 cells after P-BAP treatment. The data were expressed by mean  $\pm$  SD. Compared to the control, \*\* $p < 0.01$  represented highly significant difference.

the concentration of 3.12  $\mu\text{mol/L}$  (low dose), 6.25  $\mu\text{mol/L}$  (medium dose) and 12.5  $\mu\text{mol/L}$  (high dose), causing an obvious decrease in ATP production accordingly (Fig. 4D).

### 3.5. P-BAP could treat HCC in tumor-bearing mice

After subcutaneous transplantation of liver cancer H22 cells, the cells proliferated rapidly and the tumor volume in model group increased with days. Although the tumor volume in cisplatin-treated mice reduced, the animals were thin and weak with sparse hair and loss of activity. However, the mice in P-BAP-treated group were in good condition with normal diet and activities. The statistical results showed that the mouse weight in cisplatin-treated group was significantly lower than other groups, while there was no difference between P-BAP-treated group and model group (Fig. 5A).

All mice were euthanized and tumor tissues were dissected out respectively when tumor volume in model group grew to 3.0  $\text{cm}^3$ . The tumor mass in model group displayed pink with vascular distribution, while the color became pale in P-BAP-treated group. Notably, after mice were given 5 mg/kg P-BAP administration for 10 days, the subcutaneous tumor of one mouse completely disappeared (1/8); and when the dose increased to 10 mg/kg, the tumor volume was smaller than other groups, and the tumors in two mice totally degraded (2/8) (Fig. 5B). The result of tumor weight showed that the weight in P-BAP-treated mice was significantly decreased in a dose-dependent manner (Fig. 5C). The tumor inhibition rate were respectively 55.4% (2.5 mg/kg P-BAP group), 75.1% (5 mg/kg P-BAP group) and 85.5% (10 mg/kg P-BAP group), higher than 10 mg/kg cisplatin-treated mice

(33.4%). The results suggest that P-BAP can significantly inhibit tumor growth and even completely eliminate tumor *in vivo*.

After HE staining, it's observed that the tumor tissue in model group filled with tumor cells under the optical microscope, but the number of tumor cells on sections decreased significantly with the increase of P-BAP dose (Fig. 5D). The images of TUNEL staining showed that a large number of apoptosis-positive cells exhibited in the tumor tissue of P-BAP-treated group, and the apoptotic cells elevated with the increase of P-BAP dose (Fig. 5D), indicating that P-BAP inhibited the tumor growth by inducing tumor cell apoptosis.

### 3.6. Histological observation on inhibition of tumor growth by P-BAP

Since P-BAP has the ability of complete removal of tumor mass, the tumor histomorphology was observed in P-BAP-treated group and model group. There were blood vessels distributed on the surface and inside of the tumor tissue in model group, so that the tumor showed sufficient blood supply (Fig. 6A). However, no obvious vascular distributed in the tumor after P-BAP administration, and the interior of the tumor became hollow (Fig. 6A). Moreover, tumor sections of model group exhibited dense structure filled with tumor cells, but the sections in P-BAP-treated group appeared hollow (Fig. 6B). With the increase of P-BAP dose, the numbers of nucleus staining (blue) became less and hollow area larger, indicating that the number of surviving cells decreased.

Under microscope, it could be observed that there were few intact cells between parenchymal and hollow structure in P-

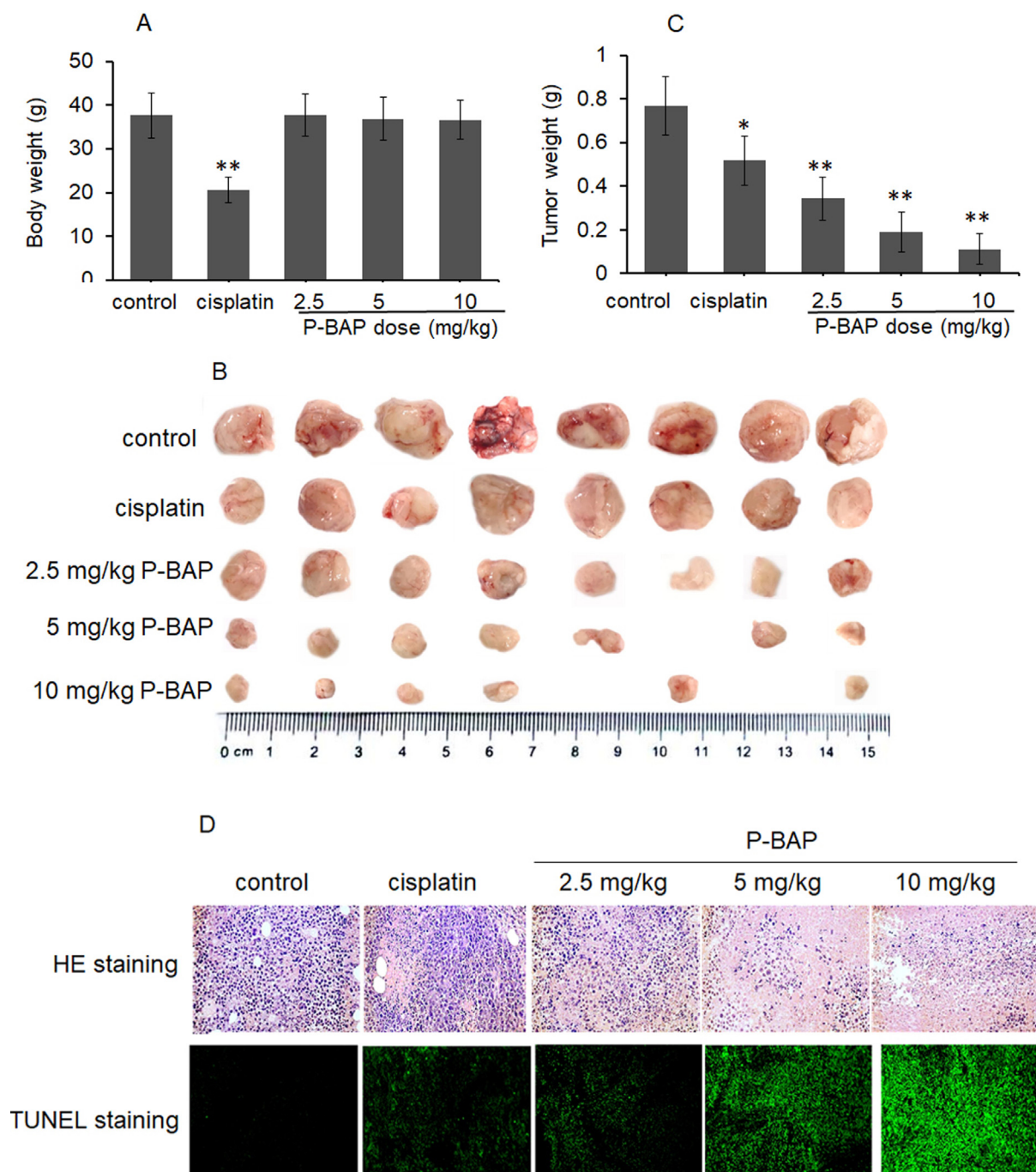


**Fig. 5** P-BAP could inhibit tumor growth in the tumor-bearing mice. (A) Mouse body weight ( $n = 8$  in each group). (B) Tumor mass in each group. (C) Tumor weight. The data were expressed by mean  $\pm$  SD. Compared to control,  $*p < 0.05$  represented significant difference, and  $**p < 0.01$  referred to highly significant difference between groups. (D) HE and TUNEL staining in tumor tissue.

BAP-treated group, and intercellular adhesion became broken, meanwhile a large number of apoptotic cells appeared (Fig. 6C). After comparing tumor sections of P-BAP-treated group and model group, it was found that the tumor cells in model group were densely distributed in tumor mass, but cell fragments without nuclear staining located around the tumor blood vessels in P-BAP-treated group. TUNEL staining also showed numbers of apoptotic cells around blood vessels (Fig. 6D). Both the cell fragment area and apoptosis-positive cells elevated following the increase of P-BAP dose. The results

indicated that P-BAP could induce tumor cell apoptosis after penetrating the blood vessels.

### 3.7. Molecular mechanism of P-BAP inhibiting tumor growth

The tumor tissues were taken for WB analysis of PLAGL2, HIF-1 $\alpha$ ,  $\beta$ -catenin, BNIP3 and BAX. The result was shown in Fig. 7. Compared with model control, the protein levels of PLAGL2, HIF-1 $\alpha$  and  $\beta$ -catenin in P-BAP-treated group reduced significantly in a dose-dependent manner (Fig. 7A-

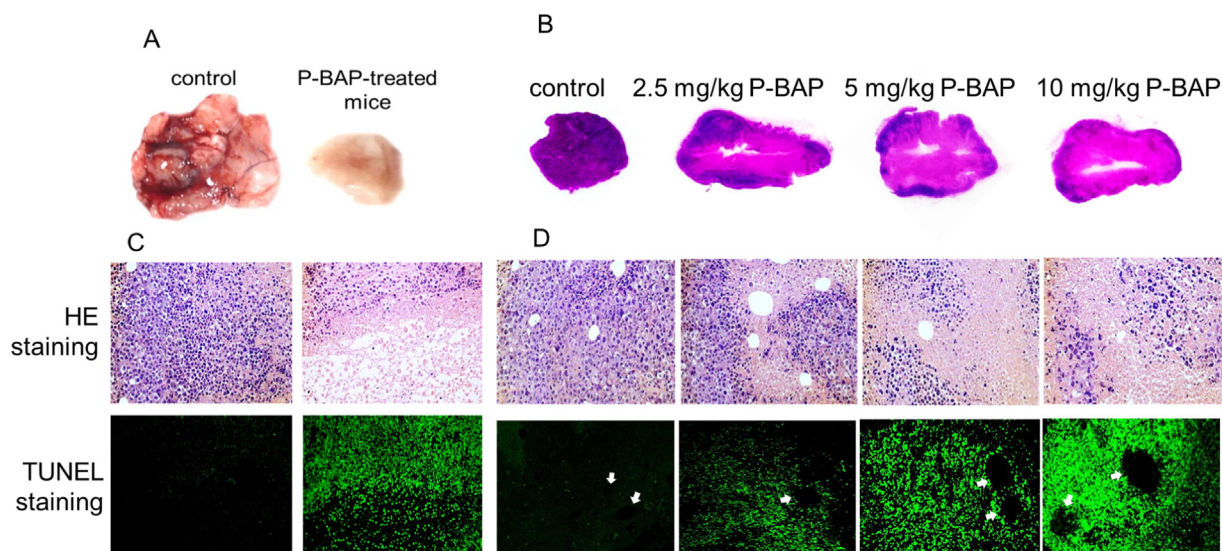


**Fig. 6** P-BAP could penetrate blood vessels and induce tumor cell apoptosis, resulting in cavitation in tumor tissue. (A) Representative tumor mass in model group and P-BAP-treated group. (B) Tumor tissue sections of each group. (C) Intercellular adhesion broken and apoptosis-positive cells appeared after P-BAP administration, evaluated by HE and TUNEL staining. (D) P-BAP penetrated blood vessels to induce tumor cell apoptosis. The arrows pointed to the vessels.

D), while the contents of pro-apoptotic proteins BNIP3 and Bax obviously increased (Fig. 7E and 7F). Moreover, activities of mitochondrial respiratory chain complex I, II, IV reduced significantly (Fig. 7G-I), resulting in the decrease of energy production accordingly (Fig. 7J).

#### 4. Discussion

The incidence and mortality of HCC continues to increase rapidly in recent years. The therapeutic goal of advanced HCC is to control tumor cell proliferation, increase survival, and maintain quality of life. Therefore, the basic principle of designing and synthesizing the antitumor drugs is to selectively kill tumor cells, without affecting the function of normal cells. In this study, hydrogen-bonded P-BAP was successfully synthesized by intermolecular proton transfer reaction, and both cell experiment and *in vivo* study proved that P-BAP could selectively inhibit the proliferation of tumor cells. Its molecular mechanism of inhibiting HCC would be associated to down-regulate the expression of PLAGL2 and its related molecules, including HIF-1 $\alpha$  and  $\beta$ -catenin, and meanwhile reduce mitochondrial respiratory chain complex activity, leading to the tumor cell apoptosis.

Previous studies suggest that two types of strong hydrogen bonds, low-barrier hydrogen bond and single-well hydrogen bond, can be produced under certain reaction conditions (Klinman, 2015). For example, Alder et al. report that diamines on 1,8-bis(dimethylamino)naphthalene (DMAN) possess proton accepting ability (“proton sponge”), forming a protonated low-barrier hydrogen bond (N-H<sup>+</sup>...N) (Alder et al., 1968; Ozeryanskii et al., 2021). Afterwards, evidence of proton sponge of intramolecular protonated hydrogen bond are rapidly increased (Lucjan et al., 2016; Majerz and Olovsson, 2009). However, few studies report the formation of strong intermolecular protonated hydrogen bond, which would be more important in revealing biomolecule interactions and designing drugs. Recently a dimeric histidine (H-bihistidine)

containing protonated hydrogen bond (N-H<sup>+</sup>...N) that is synthesized by intermolecular proton transfer is reported, in which the H-bihistidine exhibits high activity as a free radical scavenger (Zhao et al., 2021). In this study, 5-amino-1,10-phenanthroline also can form a stable protonated P-BAP by accepting a proton from ammonium salt, speculating that the hydrogen bond formed between 5-amino-1,10-phenanthroline was a low-barrier hydrogen bond with high bond energy.

Here P-BAP exhibits selective antitumor activity *in vitro* and *in vivo*, thus the molecular mechanism is explored in the study. It's known that PLAGL2 acts as an oncogene in various malignant tumors, which is closely related to tumor occurrence and development, invasion, metastasis, drug resistance and poor prognosis (Hu et al., 2020; Strubberg et al., 2018). PLAGL2 can also regulate many genes involved in tumor proliferation, angiogenesis and tumor metastasis. Increasing evidence suggests that PLAGL2 is highly expressed in HCC, gastric cancer, colon cancer, lymphoma, neuroblastoma, prostate cancer, lung cancer and other tumor cells (Cao et al., 2021; Su et al., 2018), but low or even no expression in normal cells (Liu et al., 2014; Wang et al., 2022). In HCC, PLAGL2 is up-regulated compared with non-tumorous cells. PLAGL2 can promote HCC cell proliferation, migration, and invasion (Hu et al., 2021). And also, PLAGL2 mediates the mitochondrial apoptosis resistance of HCC through activating the C-MET/STAT3 signal pathway (Yang et al., 2021). Down-regulation of PLAGL2 can inhibit tumor cells proliferation and induce the cell apoptosis (Gao and Ye, 2020; Yang et al., 2021). Since PLAGL2 is a differentially expressed transcription factor of tumor cells, it's considered that PLAGL2 is a potential target in tumor therapy (Li et al., 2020).

In this study, P-BAP shows the capability to significantly down-regulate the expression level of PLAGL2 protein at 30 min after addition to cell media. Among the downstream genes regulated by PLAGL2, HIF-1 $\alpha$  and  $\beta$ -catenin are two typical proteins closely related to tumor development and

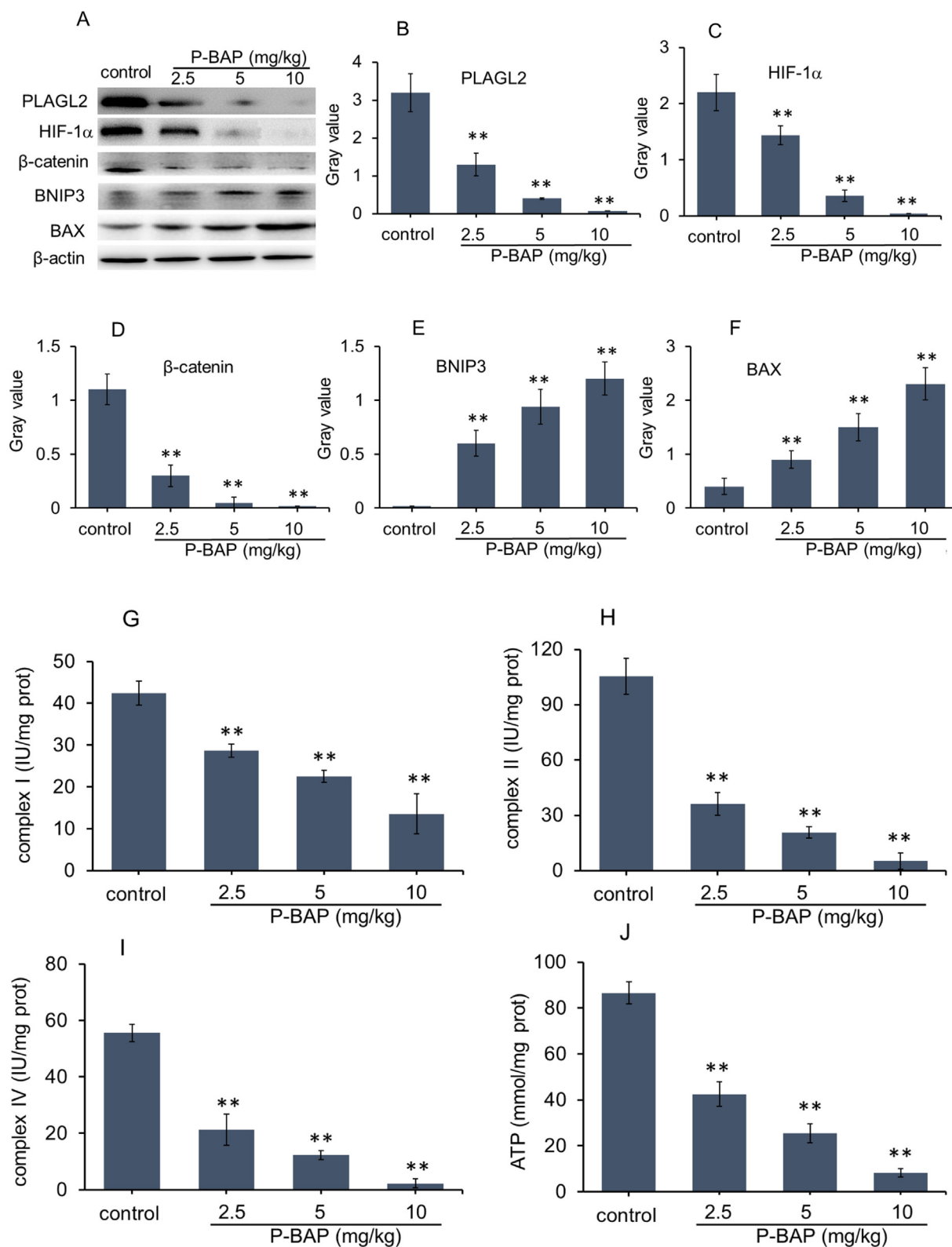


**Fig. 7** Mechanism of P-BAP inhibiting tumor growth in tissues. (A) WB analysis. (B-F) Ratio of gray value of PLAGL2, HIF-1α, β-catenin, BNIP3 and BAX. Compared to control, \* $p < 0.05$  represented significant difference, and \*\* $p < 0.01$  highly significant difference. (G-I) Activities of mitochondrial respiratory chain complex I, II, IV. (J) ATP content. The mouse number of each group was 6 ~ 8 ( $n = 6 \sim 8$ ). The data were expressed by mean  $\pm$  SD. Compared to model control, \* $p < 0.05$  represented significant difference, and \*\* $p < 0.01$  referred to highly significant difference.

malignancy. HIF is a hypoxia-inducible protein overexpressed in hypoxic microenvironment of tumor, which can promote the growth and proliferation of tumor cells, and meanwhile stimulate tumor angiogenesis (Yang et al., 2021). In addition,  $\beta$ -catenin is a signal transduction molecule and intercellular adhesion molecule, which plays an important role in tumor invasion and metastasis (Kim et al., 2019). Activation of PLAGL2 can up-regulate HIF-1 $\alpha$  expression through EGFR/PI3K/Akt signal pathway (Wang et al., 2021; Wu et al., 2019), and enhance  $\beta$ -catenin expression through PLAGL2/Wnt/ $\beta$ -catenin pathway (Wang et al., 2017; Wu et al., 2020). The both pathways can promote tumor cell proliferation and metastasis. Thus, down-regulation of PLAGL2 protein by P-BAP can reduce the protein levels of HIF-1 $\alpha$  and  $\beta$ -catenin, subsequently inhibit the proliferation of the tumor cells, and reduce intercellular adhesion and induce cell apoptosis.

Mitochondria are indispensable for HCC proliferation and malignancy because mitochondria provide energy and metabolic intermediates for the cells (Grasso et al., 2020; Keerthiga et al., 2021). Currently inhibition of the mitochondrial function has become an effective strategy for HCC therapy (Bian et al., 2021; Chang et al., 2019; Yu et al., 2021). In recent reports, PLAGL2 would affect mitochondrial function and regulate the mitochondrial apoptosis resistance in HCC (Yang et al., 2021; Zhao et al., 2022). In addition, PLAGL2, as a very upstream key transcription factor (Wang et al., 2017), could regulate the gene expression of mitochondrial transcription factor (TFAM) and then the activities of mitochondrial respiratory chain complexes through PLAGL2/Wnt signal pathway (Delgado-Deida et al., 2020; Zheng et al., 2010). Therefore, the down-regulation of PLAGL2 by P-BAP would reduce the activities of mitochondrial respiratory chain proteins, causing insufficient energy production and subsequently tumor growth inhibition.

## 5. Conclusion

In summary, here we suggest the synthesis method of hydrogen-bonded P-BAP, and identify that the P-BAP has the capability to inhibit tumor cell proliferation and induce apoptosis through regulating the PLAGL2 expression and its downstream tumor-related proteins. This study would provide a potential candidate for HCC therapy.

## Author Contributions

Zizhen Zhao and Chen Fu were responsible for the design and synthesis of target compound. Zizhen Zhao did the cell and animal study. Yingying Zhang performed the stability of the compound. Chen Fu and Yuping Zhang did the structure identification. Xiaoxi Yang analyzed purity of the compound. Ailing Fu designed the study and manuscript calibration.

## Funding

The study was supported by National Natural Science Fund of China (82073830) and Fundamental Research Funds for the Central Universities, SWU (7110100301).

## Declaration of Competing Interest

The authors declare that they have no known competing financial interests or personal relationships that could have appeared to influence the work reported in this paper.

## Appendix A. Supplementary material

Supplementary data to this article can be found online at <https://doi.org/10.1016/j.arabjc.2022.103982>.

## References

- Adams, L.A., Roberts, S.K., Strasser, S.I., Mahady, S.E., Powell, E., Estes, C., Razavi, H., George, J., 2020. Nonalcoholic fatty liver disease burden: Australia, 2019–2030. *J. Gastroenterol. Hepatol.* 35, 1628–1635.
- Alder, R.W., Bowman, P.S., Steele, W.R.S., Winterma, D.R., 1968. The remarkable basicity of 1,8-bis(dimethylamino)naphthalene. *Chem. Comm.* 13, 723–724.
- Altieri, D.C., 2017. Mitochondria on the move: emerging paradigms of organelle trafficking in tumour plasticity and metastasis. *Br. J. Cancer* 117, 301–305.
- Anwanwan, D., Singh, S.K., Singh, S., Saikam, V., Singh, R., 2020. Challenges in liver cancer and possible treatment approaches. *Biochim. Biophys. Acta Rev. Cancer* 1873, 188314.
- Bian, J., Zhang, D., Wang, Y., Qin, H., Yang, W., Cui, R., Sheng, J., 2021. Mitochondrial quality control in hepatocellular carcinoma. *Front. Oncol.* 11, 713721.
- Cao, Y., Tao, Q., Kao, X., Zhu, X., 2021. Hsa-circRNA-103809 promotes hepatocellular carcinoma development via MicroRNA-1270/PLAG1 like zinc finger 2 axis. *Dig. Dis. Sci.* 66, 1524–1532.
- Chang, C.W., Lo, J.F., Wang, X.W., 2019. Roles of mitochondria in liver cancer stem cells. *Differentiation* 107, 35–41.
- Chen, Z., Xie, H., Hu, M., Huang, T., Hu, Y., Sang, N., Zhao, Y., 2020. Recent progress in treatment of hepatocellular carcinoma. *Am. J. Cancer Res.* 10, 2993–3036.
- Delgado-Deida, Y., Alula, K.M., Theiss, A.L., 2020. The influence of mitochondrial- directed regulation of Wnt signaling on tumorigenesis. *Gastroenterol. Rep. (Oxf.)* 8, 215–223.
- Facciorusso, A., Villani, R., Bellanti, F., Mitarotonda, D., Vendemiale, G., Serviddio, G., 2016. Mitochondrial signaling and hepatocellular carcinoma: molecular mechanisms and therapeutic implications. *Curr. Pharm. Des.* 22, 2689–2696.
- Gao, N., Ye, B., 2020. Circ-SOX4 drives the tumorigenesis and development of lung adenocarcinoma via sponging miR-1270 and modulating PLAGL2 to activate WNT signaling pathway. *Cancer Cell Int.* 20, 2.
- Grasso, D., Zampieri, L.X., Capelôa, T., Van de Velde, J.A., Sonveaux, P., 2020. Mitochondria in cancer. *Cell Stress* 4, 114–146.
- Hu, W., Zheng, S., Guo, H., Dai, B., Ni, J., Shi, Y., Bian, H., Li, L., Shen, Y., Wu, M., Tian, Z., Liu, G., Hossain, M.A., Yang, H., Wang, D., Zhang, Q., Yu, J., Birnbaumer, L., Feng, J., Yu, D., Yang, Y., 2021. PLAGL2-EGFR-HIF-1/2 $\alpha$  signaling loop promotes HCC progression and Erlotinib insensitivity. *Hepatology* 73, 674–691.
- Karas, L.J., Wu, C.H., Das, R., Wu, J.I.C., 2020. Hydrogen bond design principles. *Wiley Interdiscip. Rev. Comput. Mol. Sci.* 10, e1477.
- Keerthiga, R., Pei, D.S., Fu, A., 2021. Mitochondrial dysfunction, UPRmt signaling, and targeted therapy in metastasis tumor. *Cell Biosci.* 11, 186.
- Kim, E., Lisby, A., Ma, C., Lo, N., Ehmer, U., Hayer, K.E., Furth, E. E., Viatour, P., 2019. Promotion of growth factor signaling as a critical function of  $\beta$ -catenin during HCC progression. *Nat. Commun.* 10, 1909.

- Klinman, J.P., 2015. Low barrier hydrogen bonds: getting close, but not sharing. ... ACS Cent. Sci. 3, 115–116.
- Li, T., Mao, C., Wang, X., Shi, Y., Tao, Y., 2020. Epigenetic crosstalk between hypoxia and tumor driven by HIF regulation. *J. Exp. Clin. Cancer Res.* 39, 224.
- Liu, B., Lu, C., Song, Y.X., Gao, P., Wang, Z.N., 2014. The role of pleomorphic adenoma gene-like 2 in gastrointestinal cancer development, progression, and prognosis. *Int. J. Clin. Exp. Pathol.* 7, 3089–3100.
- Lucjan, S., Dorota, C., Tolstoy, P.M., Filarowski, A., 2016. Some brief notes on theoretical and experimental investigations of intramolecular hydrogen bonding. *Molecules* 21, 1657.
- Majerz, I., Olovsson, I., 2009. Proton transfer in the intramolecular NHN+ bonds in proton sponges with different hydrogen bridge flexibility. *Phys. Chem. Chem. Physics* 11, 1297–1302.
- Ozeryanskii, V.A., Marchenko, A.V., Pozharskii, F., 2021. Combination of “Buttressing” and “Clothespin” effects for reaching the shortest NHN hydrogen bond in proton sponge cations. *J. Org. Chem.* 4, 3637–3647.
- Strubberg, A.M., Paniagua, D.A.V., Zhao, T., Dublin, L., Pritchard, T., Bayguinov, P.O., Fitzpatrick, J.A.J., Madison, B.B., 2018. The zinc finger transcription factor PLAGL2 enhances stem cell fate and activates expression of ASCL2 in intestinal epithelial cells. *Stem Cell Report* 11, 410–424.
- Su, C., Li, D., Li, N., Du, Y., Yang, C., Bai, Y., Lin, C., Li, X., Zhang, Y., 2018. Studying the mechanism of PLAGL2 overexpression and its carcinogenic characteristics based on 3'-untranslated region in colorectal cancer. *Int. J. Oncol.* 52, 1479–1490.
- Torre, P., Aglitti, A., Masarone, M., Persico, M., 2021. Viral hepatitis: milestones, unresolved issues, and future goals. *World J. Gastroenterol.* 27, 4603–4638.
- Vladilo, G., Hassanali, A., 2018. Hydrogen bonds and life in the universe. *Life (Basel)* 8, 1.
- Wang, G., Du, W., Che, L., Gao, X., Zhao, R., Duan, J., Gu, Z., Ma, Q., 2022. High expression of PLAGL2 is associated with poor prognosis in high-grade glioma. *Front Genet.* 12, 787746.
- Wang, L., Sun, L., Liu, R., Mo, H., Liu, Q., 2021. Long non-coding RNA MAPKAPK5-AS1/PLAGL2/HIF-1 $\alpha$  signaling loop promotes hepatocellular carcinoma progression. *J. Exp. Clin. Cancer Res.* 40, 72.
- Wang, Y.P., Guo, P.T., Zhu, Z., Zhang, H., Xu, Y., Chen, Y.Z., Liu, F., Ma, S.P., 2017. Pleomorphic adenoma gene like-2 induces epithelial-mesenchymal transition via Wnt/ $\beta$ -catenin signaling pathway in human colorectal adenocarcinoma. *Oncol. Rep.* 37, 1961–1970.
- Wu, L., Yuan, W., Chen, J., Zhou, Z., Shu, Y., Ji, J., Liu, Z., Tang, Q., Zhang, X., Shu, X., 2019. Increased miR-214 expression suppresses cell migration and proliferation in Hirschsprung disease by interacting with PLAGL2. *Pediatr. Res.* 86, 460–470.
- Wu, L., Zhou, Z., Han, S., Shu, X., 2020. PLAGL2 promotes epithelial-mesenchymal transition and mediates colorectal cancer metastasis via  $\beta$ -catenin-dependent regulation of ZEB1. *Br. J. Cancer* 122, 578–589.
- Yang, T., Huo, J., Xu, R., Su, Q., Zhang, Y., 2021. Selenium sulfide disrupts the PLAGL2/C-MET/STAT3-induced resistance against mitochondrial apoptosis in hepatocellular carcinoma. *Clin. Transl. Med.* 11, e536.
- Yu, Z., Hou, Y., Zhou, W., Zhao, Z., Liu, Z., Fu, A., 2021. The effect of mitochondrial transplantation therapy from different gender on inhibiting cell proliferation of malignant melanoma. *Int. J. Biol. Sci.* 17, 2021–2033.
- Zhang, L., Fu, C., Li, J., Zhao, Z., Hou, Y., Zhou, W., Fu, A., 2019. Discovery of a ruthenium complex for the theranosis of glioma through targeting the mitochondrial DNA with bioinformatic methods. *Int. J. Mol. Sci.* 20, 4643.
- Zhao, Z., Fu, C., Zhang, Y., Fu, A., 2021. Dimeric histidine as a novel free radical scavenger alleviates non-alcoholic liver injury. *Antioxidants* 10, 1529.
- Zhao, Z., Li, X., Cui, Z., Tong, T., Zhang, Y., Zhang, Y., Yang, X., Keerthiga, R., Fu, C., Fu, A., 2022. Synthesis of hemiprotonic phenanthroline-phenanthroline+ compounds with both antitumor and antimicrobial activity. *J. Med. Chem.* 65, 2532–2547.
- Zheng, H., Ying, H., Wiedemeyer, R., Yan, H., Quayle, S.N., Ivanova, E.V., Paik, J.H., Zhang, H., Xiao, Y., Perry, S.R., Hu, J., Vinjamoori, A., Gan, B., Sahin, E., Chheda, M.G., Brennan, C., Wang, Y.A., Hahn, W.C., Chin, L., DePinho, R.A., 2010. PLAGL2 regulates Wnt signaling to impede differentiation in neural stem cells and gliomas. *Cancer Cell.* 17, 497–509.